iScience

CellPress
OPEN ACCESS

Article

Circ-CIMIRC inhibition alleviates CIH-induced myocardial damage via FbxL4-mediated ubiquitination of PINK1

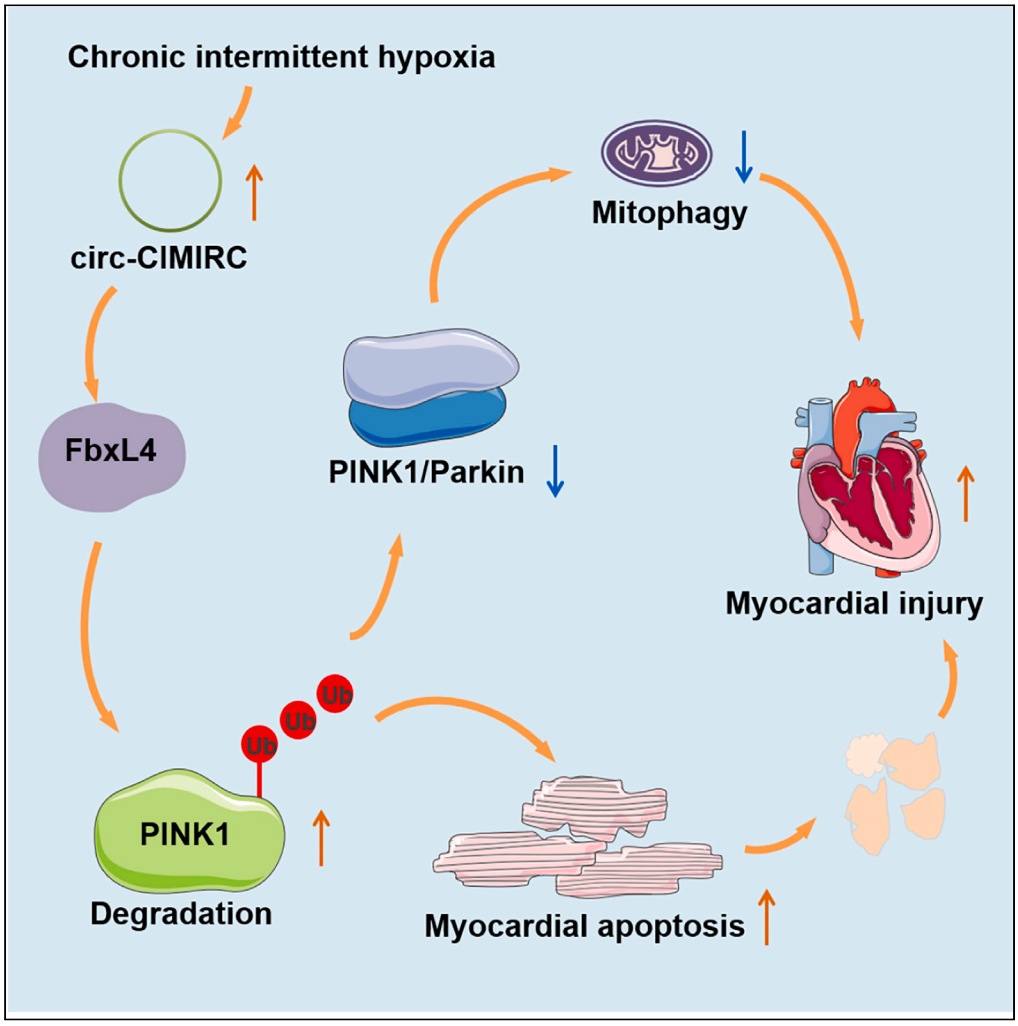

Runhua Wu, Fengsheng Xu, Jingyi Li, Feng Wang, Naijie Chen, Xiaoting Wang, Qin Chen

2014015@fjtcm.edu.cn

Highlights

FbxL4 promoted ubiquitination and degradation of PINK1 by targeting PINK1

Circ_CIMIRC inhibition alleviated CIH-induced myocardial damage in rats

Circ_CIMIRC promoted FbxL4-mediated ubiquitination and degradation of PINK1

Circ_CIMIRC silencing reduced PINK1/Parkin-mediated mitophagy

Wu et al., iScience 27, 108982
February 16, 2024
https://doi.org/10.1016/j.isci.2024.108982

iScience

CellPress
OPEN ACCESS

Article

Circ-CIMIRC inhibition alleviates CIH-induced myocardial damage via FbxL4-mediated ubiquitination of PINK1

Runhua Wu,[1,3] Fengsheng Xu,[1,3] Jingyi Li,[1] Feng Wang,[1] Naijie Chen,[1] Xiaoting Wang,[2] and Qin Chen[2,4,*]

SUMMARY

Obstructive sleep apnea (OSA) is a common sleep disordered breathing diseases that characterized by chronic intermittent hypoxia (CIH). This work aimed to explore the role of circ-CIMIRC in CIH-induced myocardial injury. CIH aggravated myocardial tissue damage in rats. Circ_CIMIRC overexpression promoted apoptosis and reduced the colocalization of Tom20 and Parkin and mitophagy in CIH-treated H9c2 cells. Additionally, FbxL4 interacted with PINK1, FbxL4 silencing reduced PINK1 ubiquitination in H9c2 cells. Two major ubiquitination sites (K319 and K433) were responsible for ubiquitination of PINK1. Circ_CIMIRC promoted FbxL4-mediated ubiquitination and degradation of PINK1. Furthermore, circ_CIMIRC inhibition alleviated the pathological damage, fibrosis and apoptosis of myocardial tissues, reduced oxidative stress in CIH rats. In conclusion, circ_CIMIRC silencing repressed FbxL4-mediated ubiquitination and degradation of PINK1 and then enhanced PINK1/Parkin-mediated mitophagy, thereby alleviating myocardial damage in CIH rats. Thus, circ_CIMIRC may be a potential strategy to alleviate CIH-induced myocardial damage.

INTRODUCTION

Obstructive sleep apnea (OSA) is a common sleep-related respiratory disorder disease, which is characterized by chronic intermittent hypoxia (CIH)-induced recurrent upper airway collapses during sleep.[1] Worldwide, OSA may affect one billion adults between the ages of thirty and sixty-nine. Moreover, it is estimated that approximately 425 million individuals suffer from moderate to severe OSA, for which medical intervention is generally recommended.[2] Clinical and animal research data indicate that OSA is a risk factor for cardiovascular injury-related pathological processes, such as systemic inflammation, oxidative stress, and endothelial dysfunction.[3,4] Studies have shown a strong correlation between intermittent hypoxia and myocardial damage resulting from OSA.[5,6] However, the molecular mechanism of myocardial injury caused by OSA is currently unclear.

FbxL4 is a nuclear encoded mitochondrial protein that controls bioenergy homeostasis and maintains mitochondrial DNA function.[7,8] A mutation in FbxL4 may cause mitochondrial fusion deficiency, indicating that FbxL4 may be involved in regulating mitophagy.[9] Abnormal expression of FbxL4 is also a risk factor for hypertrophic cardiomyopathy and arrhythmia.[10] Additionally, PINK1/Parkin pathway is one of the classical mitophagy ways to eliminate mitochondria. In order to remove damaged mitochondria, PINK1 and Parkin accumulate on the injured mitochondria and facilitate mitophagy.[11,12] Previous studies have confirmed that PINK1/Parkin pathway regulates mitophagy to selectively eliminate the damaged mitochondria in cardiomyocytes.[13,14] This approach proves to be beneficial in restoring the homeostatic imbalance of cardiomyocytes caused by hypoxia and enhancing cardiac function.[15] Moreover, a previous study has reported that CIH-induced neuroinflammation and mitochondrial reactive oxygen species (ROS) generation can be mitigated by activating mitophagy mediated by the PINK1/Parkin signaling pathway.[16] Thus, we speculated that, in CIH pathological conditions, FbxL4 may be able to modulate PINK1/Parkin-mediated mitophagy. Through STRING database, we have found that FbxL4 may interact with PINK1. UbiBrowser database have predicted that there are potential ubiquitination sites of PINK1. It suggests that FbxL4 has the ability to regulate the ubiquitination and degradation of PINK1, which is something we will investigate.

A type of non-coding RNA known as circular RNA (circRNA) serves as a bridge molecule in numerous pathophysiological processes. It is a kind of closed circRNA characterized by covalently linked 5′ and 3′ ends. Unlike traditional linear RNA, circRNAs are not easily degraded by RNA exonuclease, so they can be stably expressed. Anecdotal evidence suggests that circRNAs play an important role in cardiovascular and cerebrovascular diseases.[17,18] For instance, circ-ARF3 promotes the expression of TRAF3 through ceRNA mechanism, thereby improving mitophagy-mediated inflammation in mouse adipose tissues.[19] We speculated that circRNA may be involved in regulating Fbxl4-meidated

[1]College of Integrated Medicine, Fujian University of Traditional Chinese Medicine, Fuzhou 350100, China
[2]Clinical Skills Teaching Center, Fujian University of Traditional Chinese Medicine, Fuzhou 350100, China
[3]These authors contributed equally
[4]Lead contact
*Correspondence: 2014015@fjtcm.edu.cn
https://doi.org/10.1016/j.isci.2024.108982

mitophagy. A circRNA, circ-CIMIRC, was highly expressed in CIH rats. In this work, we sought to determine whether circ-CIMIRC could interact with PINK1 by recruiting FbxL4 to induce ubiquitination and degradation of PINK1, thereby inhibiting PINK1/Parkin-mediated mitophagy and promoting myocardial damage in CIH rats.

RESULTS

FbxL4 was upregulated, PINK1 and Parkin were downregulated in CIH rats

To investigate the precise pathogenesis of OSA, a CIH rat model was constructed to mimic OSA conditions *in vivo*. The ratio of heart weight/body weight (HW/BW) was significantly increased in CIH rats (Figure 1A). Then, hematoxylin and eosin (H&E) staining was carried out to evaluate the pathological changes of myocardial tissues. It uncovered that the pathology injury score of CIH rats was higher than that of normal rats (Figure 1B). In normal rats, myocardial cells were intact and arranged regularly. In CIH rats, a few myocardial cells were irregularly arranged. It can be seen some pathological phenomena such as cell edema, swelling, partial vasodilatation and congestion, and partial inflammatory cell infiltration. Moreover, results obtained from Masson and TUNEL staining showed that CIH rats exhibited obvious elevated myocardial fibrosis and apoptosis with respect to normal rats (Figures 1C–1E). The expression of apoptosis-related proteins was assessed by western blotting. Higher expression of cleaved-caspase-3 and p62 and decreased expression of Bcl-2 was observed in CIH rats, indicating that CIH treatment induced myocardial apoptosis in rats (Figure 1F). Previously, we carried out ITRAQ proteome sequencing and screened the differentially expressed proteins (DEGs) in myocardial tissues between CIH and normal rats. It showed that FbxL4 was abnormally upregulated in the myocardial tissue of CIH rats (Figure 1G). Also, FbxL4 was upregulated in myocardial tissues of CIH rats, suggesting that it may participate in the progression of OSA (Figure 1H). Moreover, downregulation of mitophagy-related proteins PINK1 and Parkin was observed in myocardial tissues of CIH rats (Figure 1I). The levels of PINK1 ubiquitination was elevated in CIH rats (Figure 1J), as determined by western blotting. These findings revealed that FbxL4 was upregulated, PINK1 and Parkin were downregulated in CIH rats.

FbxL4 overexpression promoted apoptosis and inhibited mitophagy in CIH-treated H9c2 cells

To validate the biological role of FbxL4 in OSA, FbxL4 was overexpressed or silenced in H9c2 cells. FbxL4 was upregulated in CIH-treated H9c2 cells following transfection of pcDNA-FbxL4. Transfection of si-FbxL4 led to a downregulation of FbxL4 in CIH-treated H9c2 cells (Figures 2A and 2B). Moreover, TUNEL staining uncovered that CIH-induced apoptosis of H9c2 cells was further accelerated by FbxL4 upregulation, whereas repressed by FbxL4 deficiency (Figure 2C). Then, to test if FbxL4 affect mitophagy of H9c2 cells, IF staining and western blotting were carried out to examine the levels of mitophagy-related proteins. As shown Figures 2D and 2E, the levels of GFP-LC3 puncta, LC3-II/LC3-I and Mfn2 were decreased in CIH-treated H9c2 cells. Upregulation of Drp1 was observed in CIH-treated H9c2 cells. FbxL4 overexpression downregulated the number of GFP-LC3 puncta, LC3-II/LC3-I and Mfn2, and upregulated Drp1 in CIH-treated H9c2 cells. FbxL4 silencing caused opposite results (Figures 2D and 2E). Thus, FbxL4 overexpression promoted apoptosis and inhibited mitophagy, whereas FbxL4 silencing reduced apoptosis and accelerated mitophagy in CIH-treated H9c2 cells.

FbxL4 promoted the ubiquitination and degradation of PINK1 by interacting with PINK1

Using STRING database, we found that FbxL4 may interact with PINK1 (Figure 3A). UbiBrowser revealed that there were potential ubiquitination sites of PINK1 (Figure 3B). To verify the relationship between FbxL4 and PINK1, we carried out co-immunoprecipitation (co-IP) assay. It showed that FbxL4 interacted with PINK1 (Figure 3C). FbxL4 silencing enhanced PINK1 expression and reduced the levels of PINK1 ubiquitination in H9c2 cells (Figures 3D–3F). Moreover, MG132 treatment reversed FbxL4 deficiency-mediated downregulation of PINK1 and promotion of PINK1 ubiquitination in H9c2 cells (Figures 3G and 3H). To comprehensively identify monoubiquitination sites on PINK1, we mutated each of 6 lysine (K; K267, K319, K369, K433, K458, and K496) residues to arginine (R). Ubiquitination assay using single K-to-R mutants of PINK1 showed that the ubiquitination levels of PINK1 were notably decreased following K-to-R mutant on K319 and K433 sites. Following K to-R mutant on K267, K369, K458, and K496 sites, the ubiquitination levels of PINK1 remained unchanged (Figure S1). It implicated that the K319 and K433 were candidates for major mono-ubiquitination sites of PINK1, other K residues were unlikely to be major ubiquitination sites. Taken together, these data implied that FbxL4 promoted the ubiquitination and degradation of PINK1 by interacting with PINK1.

Circ_CIMIRC promoted apoptosis and repressed mitophagy of CIH-treated H9c2 cells

Previously, we conducted RNA immunoprecipitation (RIP) assay and screened several circRNAs that targeting FbxL4, including circ_001863, circ_CIMIRC, circ_012098 and circ_004905. Among them, circ_CIMIRC and circ_004905 were highly expressed in CIH-treated H9c2 cells and myocardial tissues of CIH rats, especially circ_CIMIRC (Figures S2A and S2B). Then, we selected circ_CIMIRC for further investigation. Circ_CIMIRC was overexpressed or knocked down in H9c2 cells to determine the precise mechanism of circ_CIMIRC in regulating apoptosis and mitophagy of CIH-treated H9c2 cells (Figure S3). Using a TUNEL staining, we found that circ_CIMIRC overexpression enhanced apoptosis of CIH-treated H9c2 cells. Circ_CIMIRC silencing reduced apoptosis of CIH-treated H9c2 cells (Figure 4A). Results of western blotting showed that circ_CIMIRC had no influence on FbxL4 expression in CIH-treated H9c2 cells (Figure 4B). The expression of mitophagy-related proteins PINK1 and Parkin was inhibited by circ_CIMIRC overexpression, and upregulated by circ_CIMIRC inhibition in CIH-treated H9c2 cells (Figures 4C and 4D). Moreover, circ_CIMIRC overexpression reduced the expression of LC3-II/LC3-I and Mfn2 and elevated Drp1 expression

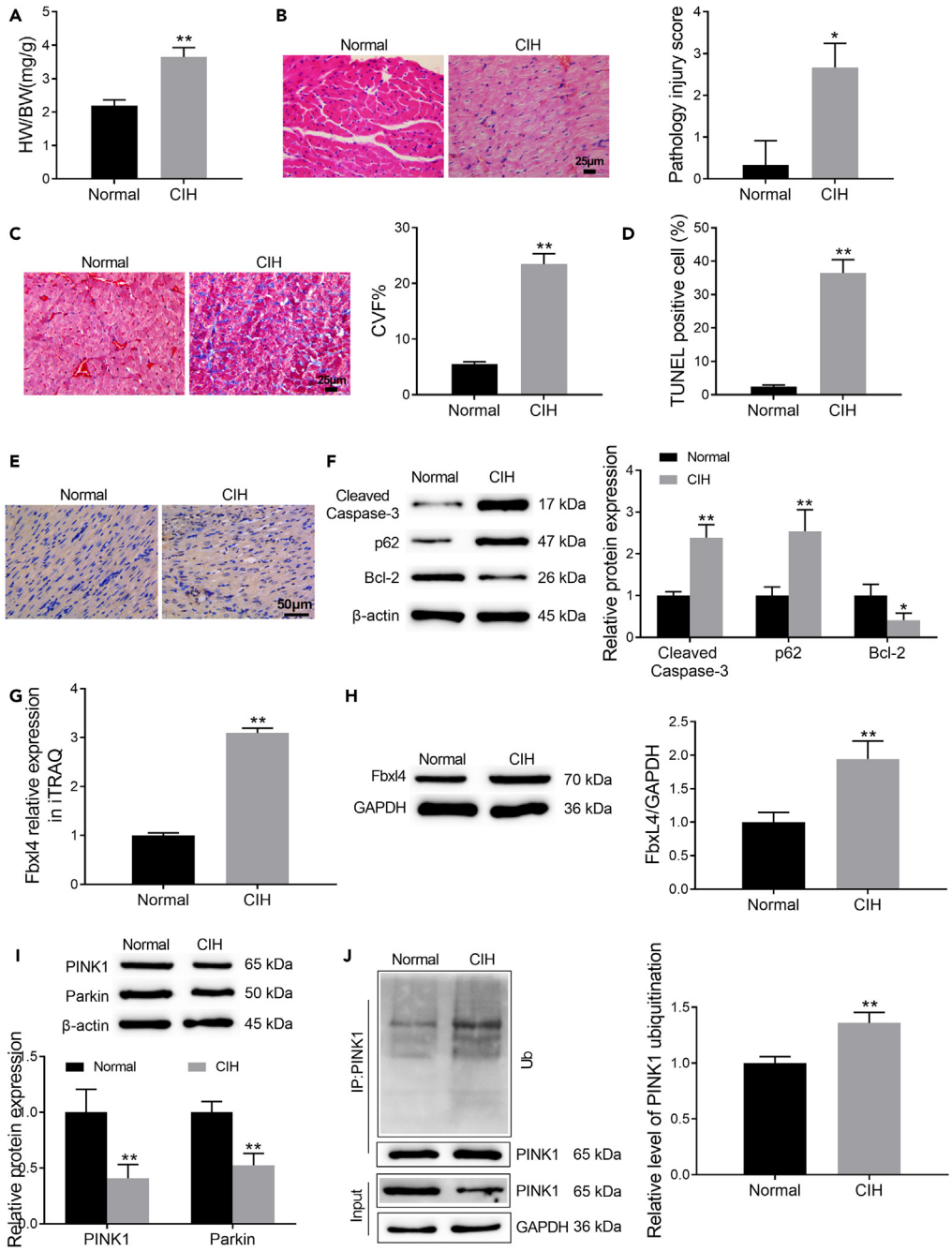

Figure 1. FbxL4 was upregulated, PINK1 and Parkin were downregulated in CIH rats

(A) Heart weight/body weight of CIH and normal rats. H&E (B), Masson (C), and TUNEL (D and E) staining assessed the pathological changes, fibrosis and apoptosis of myocardial tissues in CIH and normal rats.

(F) Western blotting examined the expression of cleaved caspase-3, p62 and Bcl-2 in myocardial tissues of CIH and normal rats.

(G) The expression of FbxL4 in iTRAQ quantification.

(H and I) Western blotting detected FbxL4, PINK1, and Parkin expression in myocardial tissues of CIH and normal rats.

(J) Western blotting assessed the levels of PINK1 ubiquitination in myocardial tissues of CIH and normal rats. *$p < 0.05$, **$p < 0.01$ vs. Normal group.

in CIH-treated H9c2 cells. Circ_CIMIRC deficiency caused opposite results (Figures 4E–4G). Furthermore, the colocalization of Parkin and Tom20 was decreased in CIH-treated H9c2 cells with circ_CIMIRC upregulation. Circ_CIMIRC silencing elevated the colocalization of Parkin and Tom20 in CIH-treated H9c2 cells, as determined by IF staining (Figure 4H). Thus, circ_CIMIRC overexpression promoted apoptosis and reduced mitophagy of CIH-treated H9c2 cells.

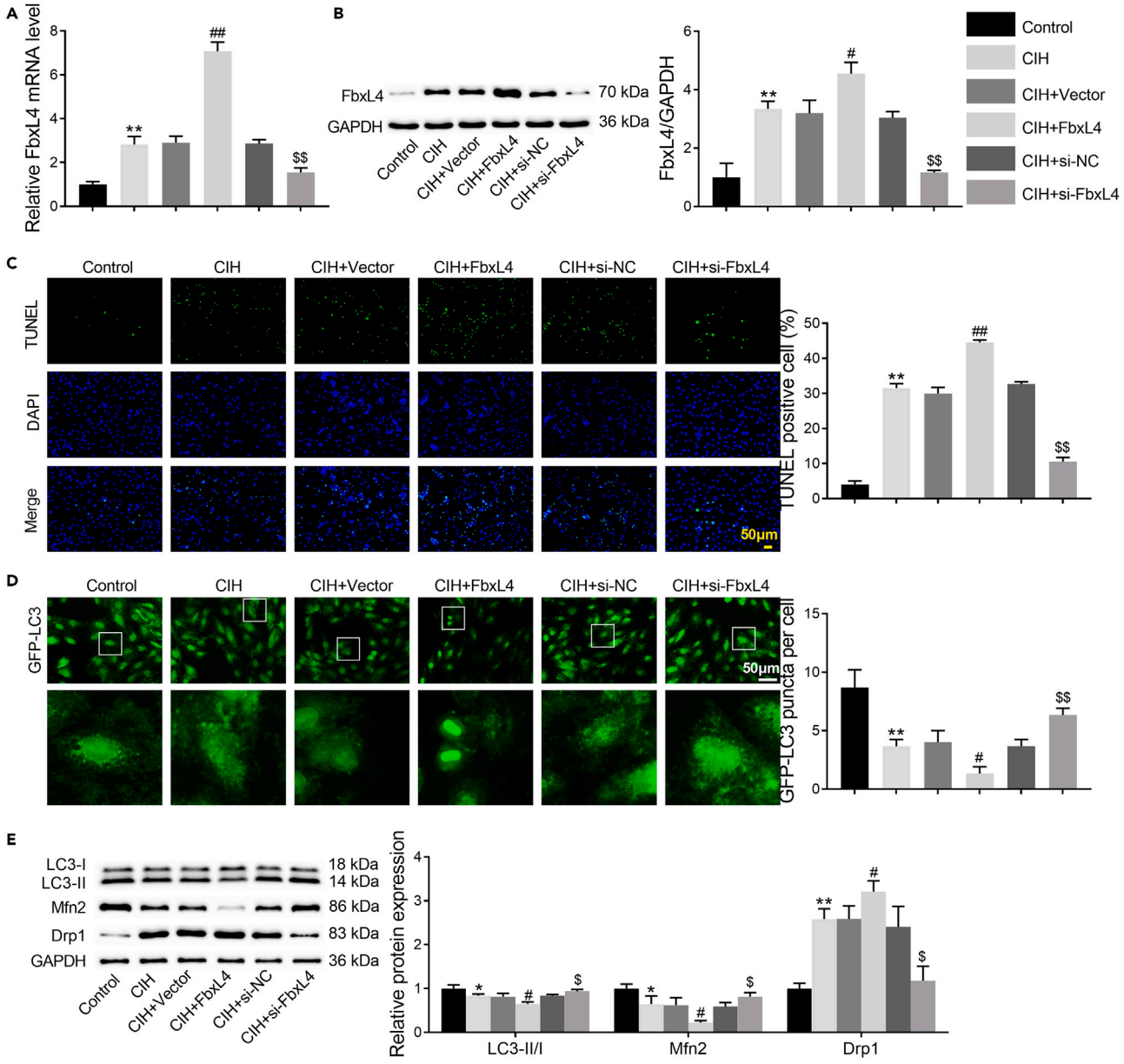

Figure 2. FbxL4 regulated apoptosis and mitophagy in CIH-treated H9c2 cells

H9c2 cells were subjected to CIH treatment, and then transfected with pcDNA-FbxL4, Vector, si-FbxL4 or si-NC. qRT-PCR (A) and western blotting (B) detected the expression of FbxL4 in H9c2 cells.

(C) TUNEL staining examined cell apoptosis.

(D) IF staining assessed the levels of GFP-LC3 puncta.

(E) Western blotting assessed the expression of LC3-I, LC3-II, Mfn2, and Drp1 in H9c2 cells. *$p < 0.05$, **$p < 0.01$ vs. Control; $^{\#}p < 0.05$, $^{\#\#}p < 0.01$ vs. CIH+Vector; $^{\$}p < 0.05$, $^{\$\$}p < 0.01$ vs. CIH+si-NC.

Circ_CIMIRC promoted FbxL4-mediated ubiquitination of PINK1

We examined the expression of circ_CIMIRC in H9c2 cells by quantitative real-time PCR (qRT-PCR). Compared with nuclear fraction, circ_CIMIRC was upregulated in cytoplasmic fraction of H9c2 cells (Figure 5A). It showed that circ_CIMIRC was mainly located in cytoplasmic of H9c2 cells. RIP assay was conducted to verify the interaction among circ_CIMIRC, FbxL4 and PINK1. The expression of circ_CIMIRC was notably increased in anti-FbxL4 and anti-PINK1 groups, indicating that circ_CIMIRC interacted with both FbxL4 and PINK1 (Figures 5B and 5C). Ubiquitination assay revealed that knockdown of circ_CIMIRC reduced the levels of PINK1 ubiquitination

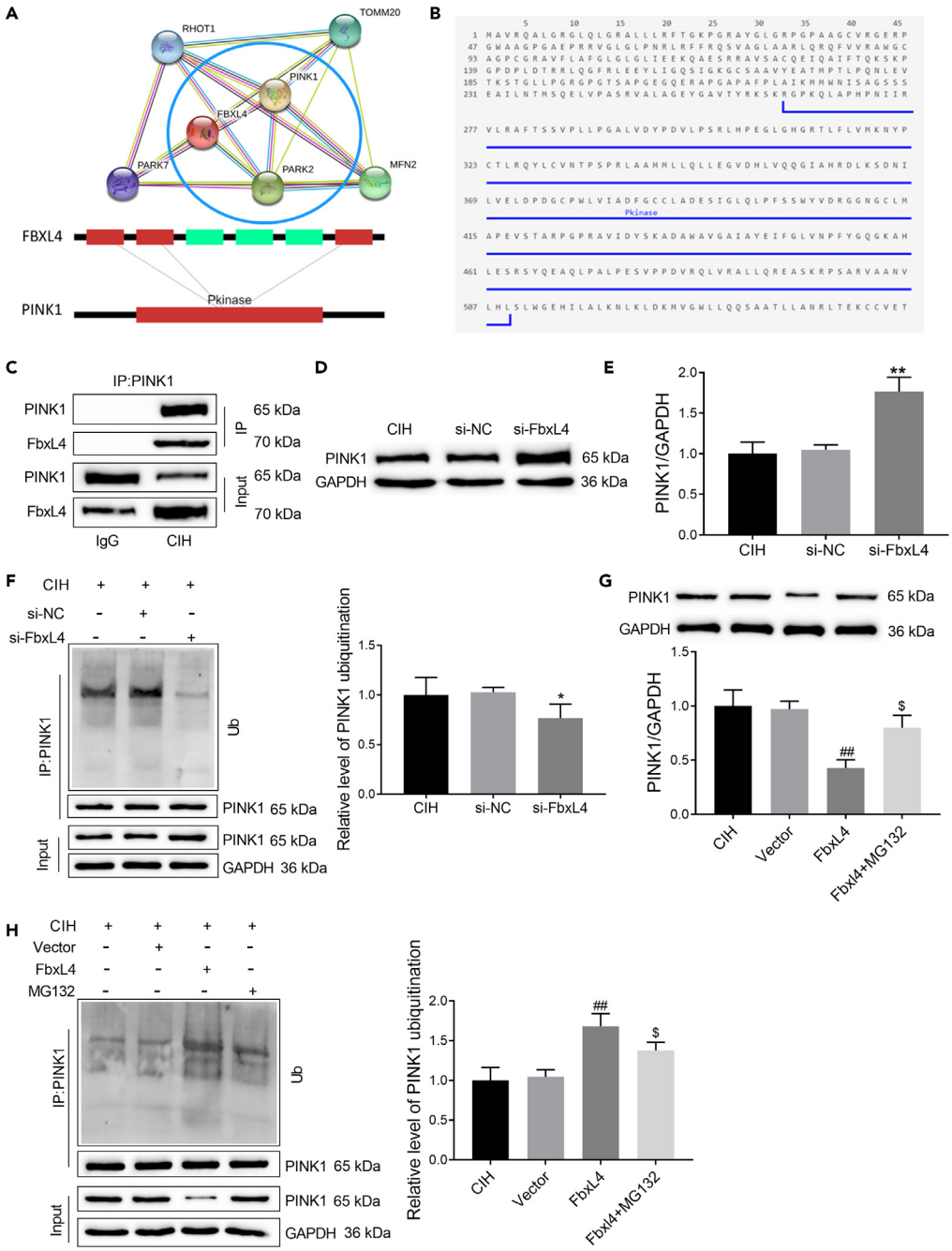

Figure 3. FbxL4 interacted with PINK1, and FbxL4 silencing inhibited the ubiquitination and degradation of PINK1

(A) STRING predicated the interaction between FbxL4 and PINK1.

(B) UbiBrowser uncovered the potential ubiquitination sites of PINK1.

(C) Co-IP verified the interaction between FbxL4 and PINK1.

(D–F) Western blotting examined the levels of PINK1 and PINK1 ubiquitination in H9c2 cells in the presence of si-NC or si-FbxL4.

(G and H) Western blotting detected the levels of PINK1 and PINK1 ubiquitination in H9c2 cells in the presence of pcDNA-FbxL4, Vector, and MG132. *$p < 0.05$, **$p < 0.01$ vs. si-NC; $^{\#}p < 0.05$, $^{\#\#}p < 0.01$ vs. Vector; $^{\$}p < 0.05$ vs. FbxL4.

in CIH-treated H9c2 cells (Figure 5D). Proteasome inhibitor, MG132, reversed circ_CIMIRC overexpression-mediated increase levels of PINK1 ubiquitination in CIH-treated H9c2 cells (Figure 5E). It indicated that circ_CIMIRC promoted FbxL4-mediated ubiquitination of PINK1.

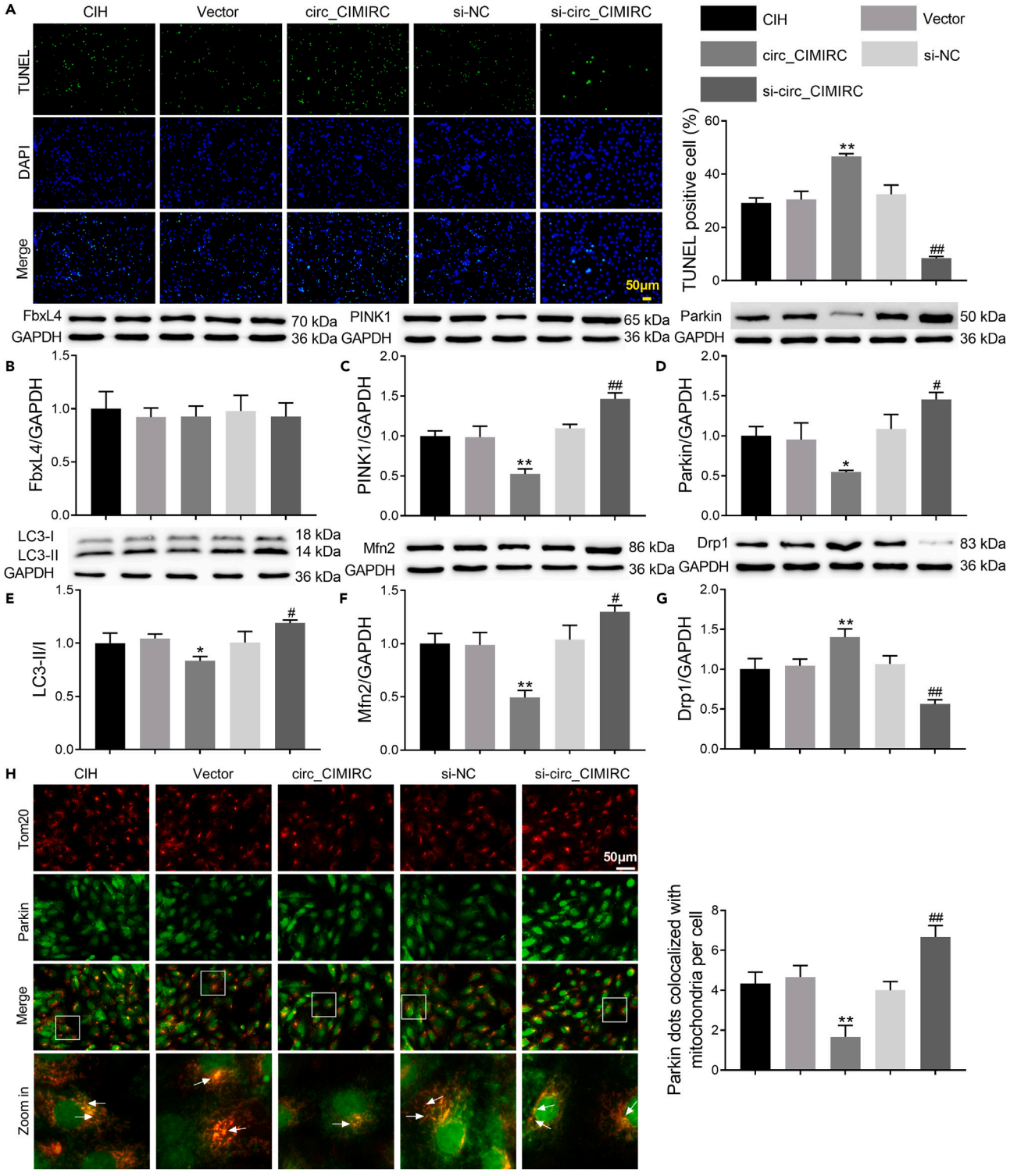

Figure 4. Circ_CIMIRC repressed PINK1 and Parkin expression, and affected apoptosis and mitophagy of CIH-treated H9c2 cells

H9c2 cells were subjected to CIH treatment, and then transfected with pcDNA-circ_CIMIRC, Vector, si-circ_CIMIRC, or si-NC.

(A) TUNEL staining examined cell apoptosis.

(B–G) Western blotting assessed the expression of FbxL4, PINK1, Parkin, LC3-I, LC3-II, Mfn2, and Drp1 in H9c2 cells.

(H) IF staining examined the levels of mitophagy in H9c2 cells. *p < 0.05, **p < 0.01 vs. Vector; #p < 0.05, ##p < 0.01 si-NC.

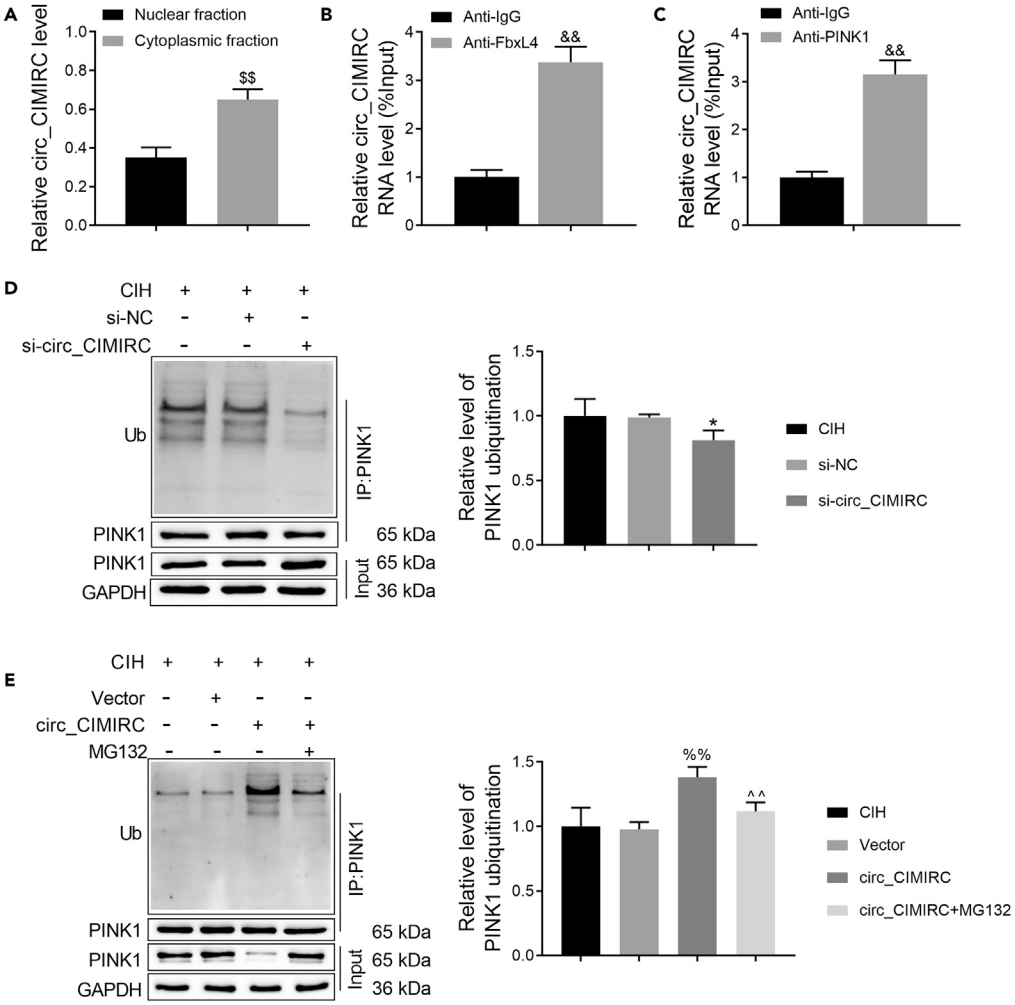

Figure 5. Circ_CIMIRC interacted with FbxL4 and PINK1, and promoted ubiquitination of PINK1

(A) qRT-PCR detected the expression of circ-CIMIRC in the cytoplasm and nucleus of H9c2 cells. $^{\$\$}p < 0.01$ vs. nuclear fraction.

(B and C) RIP verified the interaction among circ-CIMIRC, FbxL4 and PINK1. $^{\&\&}p < 0.01$ vs. Anti-IgG.

(D and E) Western blotting examined the levels of PINK1 and PINK1 ubiquitination in H9c2 cells. *$p < 0.05$ vs. si-NC; $^{\%\%}p < 0.01$ vs. Vector; $^{\wedge\wedge}p < 0.01$ vs. circ-CIMIRC.

Circ_CIMIRC deficiency inhibited apoptosis of CIH-treated H9c2 cells by regulating PINK1/Parkin-mediated mitophagy

H9c2 cells were treated with Mdivi-1 to inhibit mitophagy. Then, the influence of circ_CIMIRC deficiency on apoptosis and mitophagy of CIH-treated H9c2 cells was detected. Using a TUNEL staining, we found that Mdivi-1 treatment reversed circ_CIMIRC silencing-induced apoptosis of CIH-treated H9c2 cells (Figure 6A). Western blotting results uncovered that the expression of mitophagy-related proteins PINK1, Parkin and LC3-II/LC3-I was increased in CIH-treated H9c2 cells following circ_CIMIRC knockdown. The influence conferred by circ_CIMIRC down-regulation was abolished by Mdivi-1 treatment (Figures 6B–6E). Moreover, IF staining examined the location and expression of Parkin and Tom20 in H9c2 cells. The colocalization of Parkin and Tom20 was enhanced by circ_CIMIRC silencing, which was abolished by Mdivi-1 treatment (Figure 6F). Thus, circ_CIMIRC deficiency inhibited apoptosis of CIH-treated H9c2 cells by regulating PINK1/Parkin-mediated mitophagy.

Circ_CIMIRC inhibition reduced myocardial damage in CIH rats

Finally, we verified the influence of circ_CIMIRC knockdown on myocardial damage in rats. The ratio of HW/BW was increased in CIH rats, which was reduced by circ_CIMIRC silencing (Figure 7A). Following H&E staining results, we found that the pathology injury score was significantly increased in CIH rats, and reduced by circ_CIMIRC knockdown. It indicated that circ_CIMIRC knockdown ameliorated CIH-induced myocardial injury in rats (Figures 7B and 7C). The fibrosis and apoptosis of myocardial tissues was examined by Masson and TUNEL staining, showing that circ_CIMIRC deficiency reduced CIH-induced myocardial fibrosis and apoptosis in rats (Figures 7D–7G).

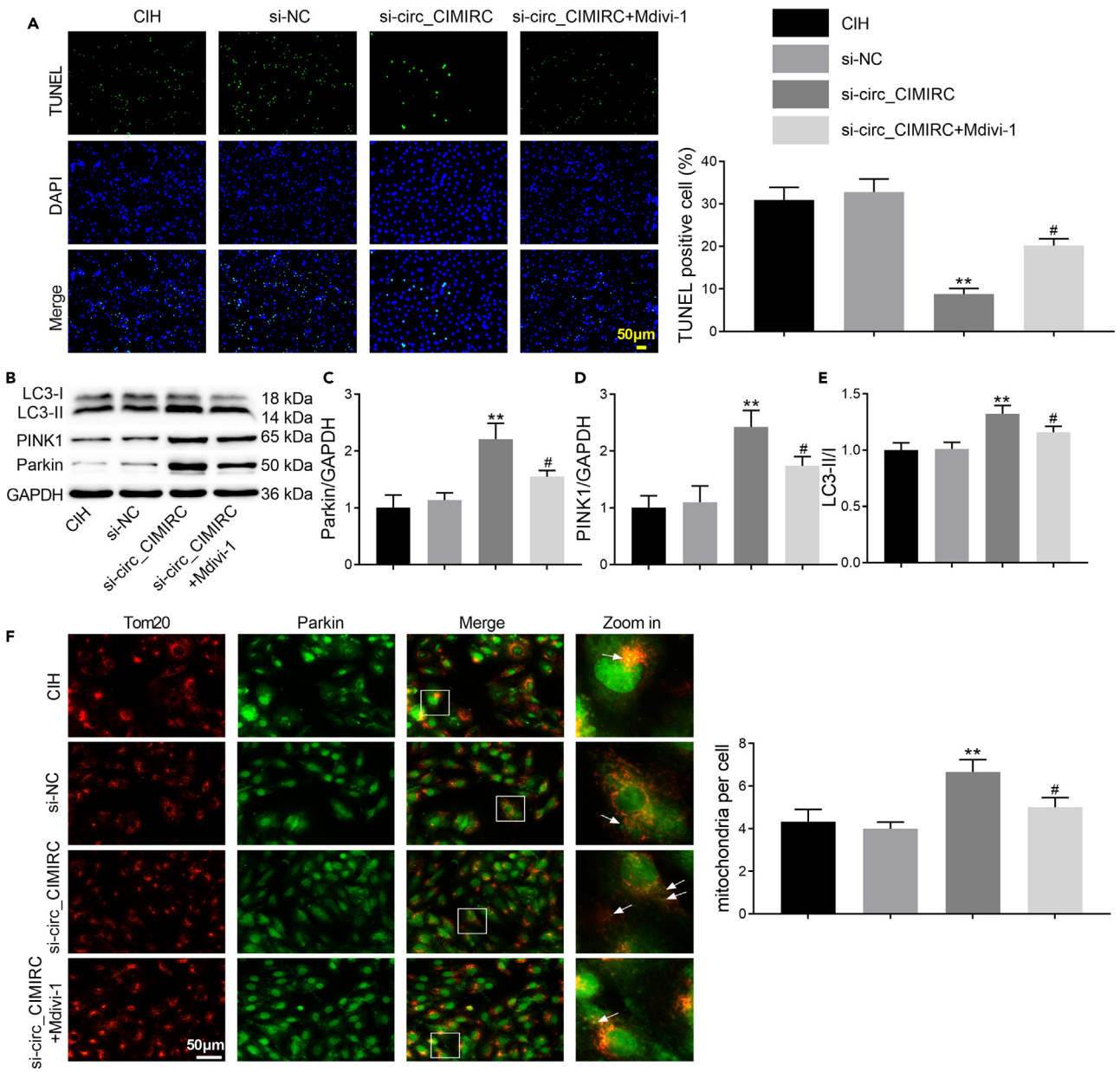

Figure 6. Circ_CIMIRC deficiency inhibited apoptosis of CIH-treated H9c2 cells by regulating mitophagy

H9c2 cells were subjected to CIH treatment, and then transfected with si-circ_CIMIRC or si-NC or combined with Mdivi-1 treatment.

(A) TUNEL staining examined apoptosis of H9c2 cells.

(B–E) Western blotting assessed the expression of PINK1, Parkin, LC3-I, and LC3-II in H9c2 cells.

(F) IF staining examined the levels of mitophagy in H9c2 cells. $^{**}p < 0.01$ vs. si-NC; $^{\#}p < 0.05$ vs. si-circ-CIMIRC.

Moreover, upregulation of cleaved-caspase-3 and p62, downregulation of Bcl-2 were observed in CIH rats. Circ_CIMIRC silencing suppressed cleaved-caspase-3 and p62 expression and elevated Bcl-2 expression in CIH rats, as determined by western blotting (Figure 7H). Additionally, circ_CIMIRC was highly expressed in CIH rats. The expression of circ_CIMIRC was decreased in CIH rats in the presence of sh-circ_CIMIRC (Figure 8A). Moreover, downregulation of PINK1, Parkin, and LC3-II/LC3-I was observed in CIH rats. Inhibition of circ_CIMIRC caused an upregulation of PINK1, Parkin, and LC3-II/LC3-I in CIH rats (Figure 8B). Immunohistochemistry (IHC) assay evaluated the expression of Fblx4 in myocardial tissues of rats, showing that Fblx4 was significantly increased in CIH rats. Circ_CIMIRC knockdown had no influence on Fblx4 expression in CIH rats (Figure 8C). In addition, the levels of oxidative stress-related markers were examined in CIH rats. CIH rats exhibited higher levels of MDA and ROS, and lower levels of SOD with respect to normal rats.

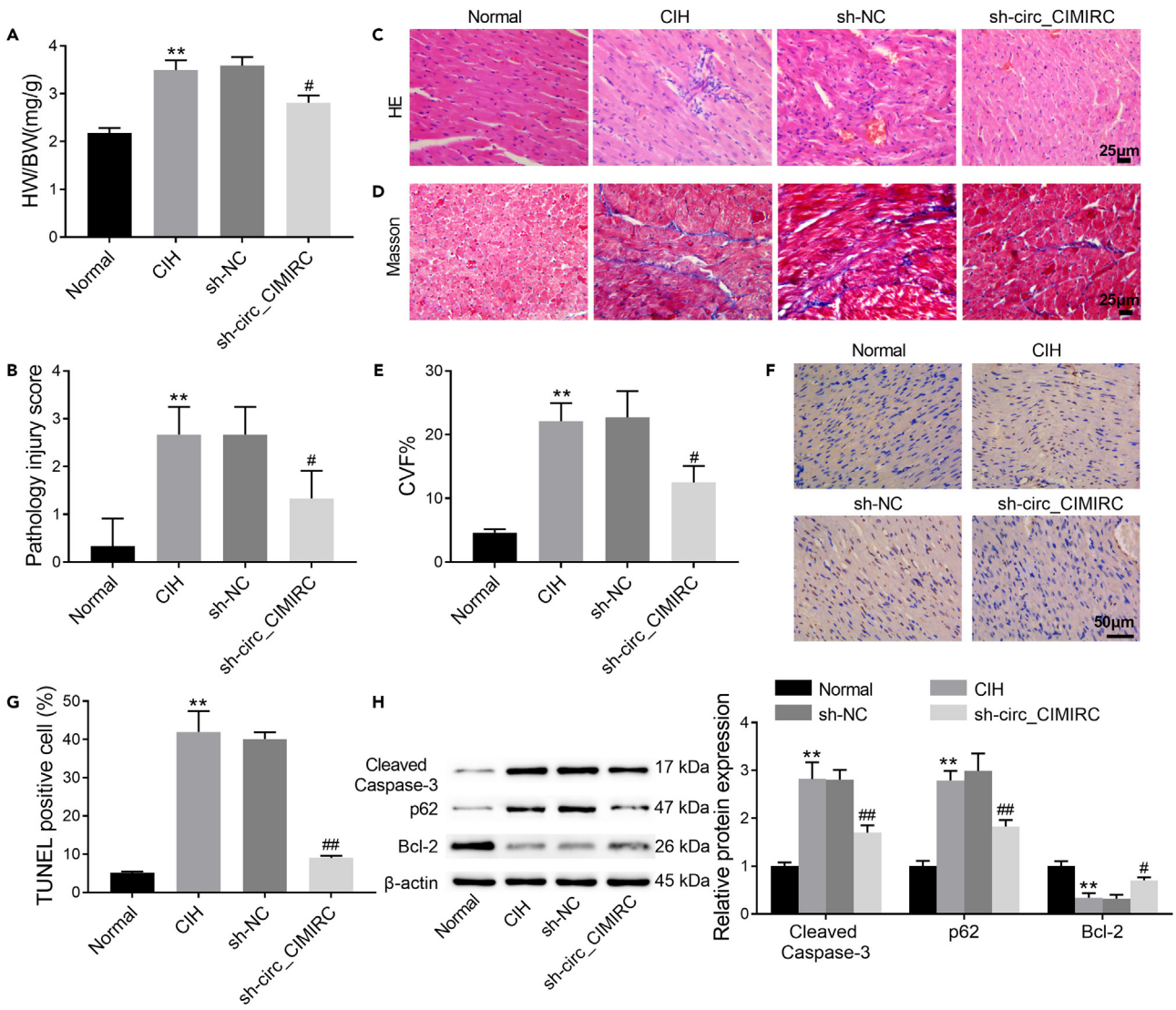

Figure 7. Circ_CIMIRC inhibition reduced myocardial damage in CIH rats

(A) Heart weight/body weight of rats. HE (B and C), Masson (D and E) and TUNEL (F and G) staining assessed the pathological changes, fibrosis and apoptosis of myocardial tissues.

(H) Western blotting examined the expression of cleaved caspase-3, p62, and Bcl-2 in myocardial tissues. **p < 0.01 vs. Normal; #p < 0.05, ##p < 0.01 vs. sh-NC.

Circ_CIMIRC silencing led to decreased levels of MDA and ROS, and increased levels of SOD in CIH rats (Figures 8D–8F). All these data suggested that circ_CIMIRC inhibition enhanced the expression of PINK1 and Parkin, and reduced myocardial damage in CIH rats.

DISCUSSION

In present study, we found that FbxL4 was upregulated, PINK1 and Parkin were downregulated in myocardial tissues of CIH rats. High levels of PINK1 ubiquitination was also observed in CIH rats. *In vitro*, FbxL4 overexpression aggravated apoptosis and alleviated mitophagy of CIH-treated H9c2 cells. Mechanism studies uncovered that FbxL4 promoted the ubiquitination and degradation of PINK1 by interacting with PINK1. Two major ubiquitination sites (K319 and K433), identified by mutational analysis with single K mutants, were responsible for ubiquitination of PINK1. Additionally, circ_CIMIRC overexpression promoted apoptosis and reduced mitophagy in CIH-treated H9c2 cells, which attributed to promote FbxL4-mediated ubiquitination and degradation of PINK1. Furthermore, circ_CIMIRC inhibition alleviated CIH-induced myocardial damage in rats. All these data indicated that circ_CIMIRC silencing repressed FbxL4-mediated ubiquitination and degradation of PINK1 and then enhanced PINK1/Parkin-mediated mitophagy, thereby alleviating myocardial damage in CIH rats.

FbxL4 has a vital role in maintaining the function of mitochondrial DNA.[20] Both systolic and diastolic function of heart is highly dependent on ATP energy metabolism. Almost all ATP in myocardial cells comes from mitochondria. Therefore, abnormal mitochondrial function leads

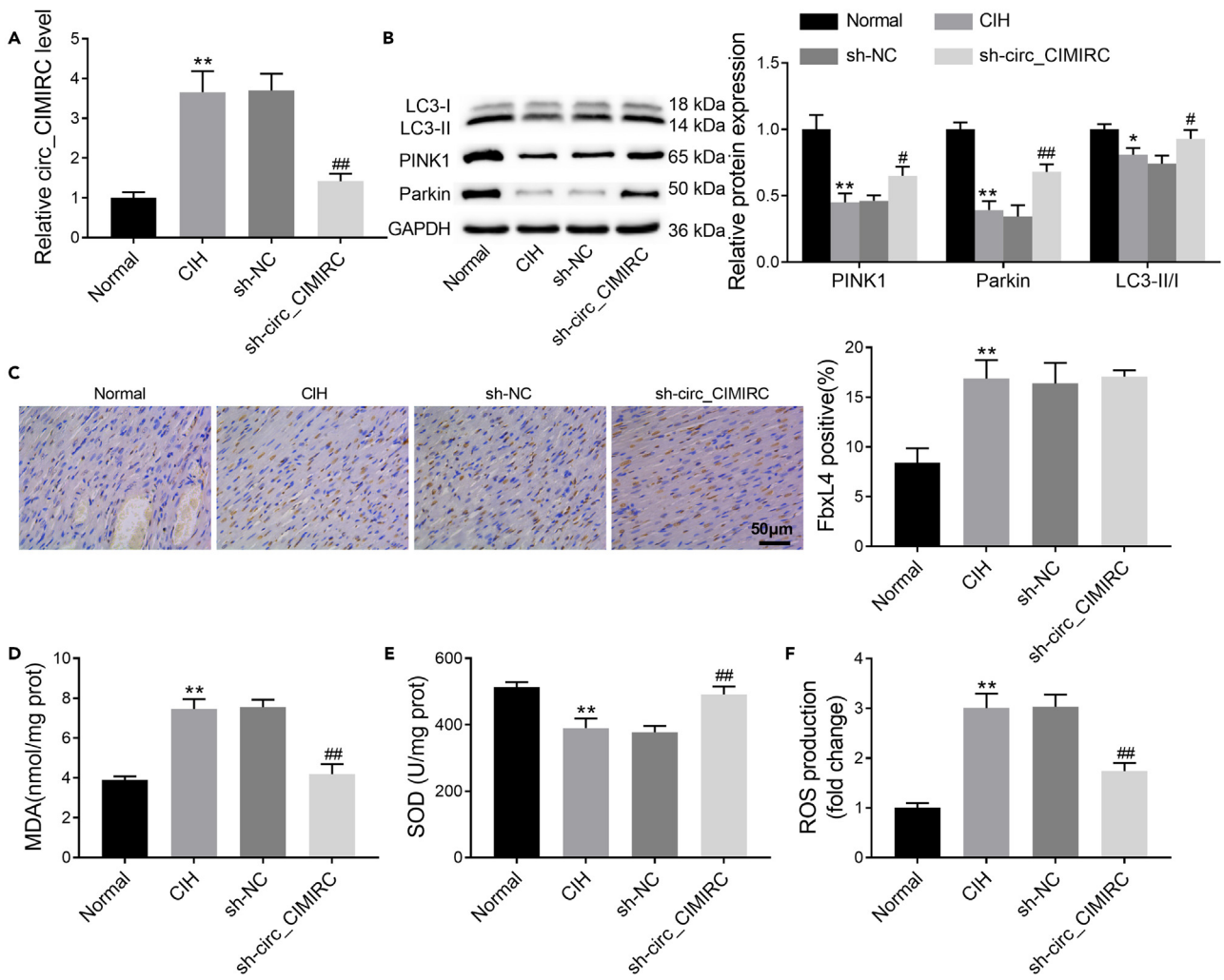

Figure 8. Circ_CIMIRC inhibition enhanced the expression of PINK1 and Parkin in CIH rats

(A) qRT-PCR detected the expression of circ-CIMIRC in myocardial tissues.

(B) Western blotting assessed the expression of PINK1, Parkin, LC3-I, and LC3-II in myocardial tissues.

(C) IHC detected the expression of FbxL4 in myocardial tissues. The levels of MDA (D), SOD (E), and ROS (F) in myocardial tissues. *$p < 0.05$, **$p < 0.01$ vs. Normal; $^{\#}p < 0.05$, $^{\#\#}p < 0.01$ vs. sh-NC.

to heart damage.[21] FbxL4 may affect heart function to participate in the pathological processes of heart diseases by regulating mitochondrial function. In the previous work, we have conducted iTRAQ proteome sequencing to screen the DEGs in the left ventricular myocardium between normal rats and CIH rats. It revealed that there are 20.24% of the mitochondrial DEGs in the myocardium of CIH rats. Among these DEGs-related to mitochondrial function, E3 ubiquitin ligase FbxL4 located on the outer membrane of mitochondria in CIH rats is 3.092 times higher than that in normal rats. In the present work, we explored the functional role of FbxL4 in CIH-induced myocardial damage. High expression of FbxL4 was observed in the CIH-induced myocardial damage rats and CIH-treated H9c2 cells. FbxL4 overexpression enhanced apoptosis and reduced autophagy in CIH-treated H9c2 cells. The mitophagy-related proteins, LC3-II/LC3-I and Mfn2 were downregulated, Drp1 was upregulated in CIH-treated H9c2 cells following FbxL4 overexpression. FbxL4 deficiency led to opposite results. Mfn2 and Drp1 are key molecules in regulating mitophagy.[22] Thus, FbxL4 promoted apoptosis and reduced mitophagy in CIH-treated H9c2 cells.

As is well known, the PINK1/Parkin signaling pathway is a classic pathway that mediates mitochondrial autophagy. It is involved in the progress of cardiac-functional diseases. For instance, MitoQ, a mitochondria-targeted antioxidant, exerts cardioprotective effects in type 2 diabetic rats with myocardial ischemia reperfusion, which attributes to activate PINK1/Parkin pathway-mediated mitophagy.[23] VDAC1 regulate PINK1/Parkin pathway to promote autophagy, thereby aggravating anoxia/reoxygenation-induced apoptosis of cardiomyocytes.[24] Qiliqiangxin, a traditional Chinese medicine compound, inhibits apoptosis of cardiomyocytes and improves heart function in myocardial infarction rats by regulating PINK1/Parkin pathway-mediated mitophagy.[25] In the present work, we observed downregulation of PINK1 and Parkin, and increased levels of PINK1 ubiquitination in CIH rats. FbxL4 silencing also repressed PINK1 ubiquitination and elevated PINK1 expression

through ubiquitination degradation pathway in CIH-treated H9c2 cells by targeting PINK1. Moreover, protein degradation controlled by ubiquitin proteasome system has important physiological significance by removing wrong proteins.[26] A previous study also confirmed that ubiquitin mediated proteolysis is closely associated with the pathogenesis of OSA.[27] MG132, as a proteasome inhibitor, reversed FbxL4-meidated PINK1 ubiquitination and degradation.

CircRNAs take part in the pathological process of various myocardial diseases. For instance, circRNA_000203 upregulates the levels of Gata4 by sponging miR-26b-5p and miR-140-3p, and then, which contributes to aggravate cardiac hypertrophy in mice.[28] Downregulation of circFndc3b is observed in cardiac tissues of post myocardial infarction mice and ischemic cardiomyopathy patients. CircFndc3b overexpression improves left ventricular functions by reducing apoptosis of cardiomyocytes and accelerating neovascularization.[29] Lai et al.[30] have screened 23 downregulated circRNAs and 101 upregulated circRNAs between CIH-induced OSA mice and normal mice through circRNA microarray. These differentially expressed circRNAs may be closely associated with CIH-induced OSA. In our previous research, we found that circ_CIMIRC can bind to FbxL4, which was highly expressed in CIH rats and CIH-treated H9c2 cells. Here, we explored the precise function of circ_CIMIRC in CIH-induced myocardial damage. We found that circ_CIMIRC upregulation enhanced apoptosis and inhibited mitophagy in CIH-treated H9c2 cells. Circ_CIMIRC promoted FbxL4-mediated ubiquitination and degradation of PINK1 by interacting with FbxL4. *In vivo*, circ_CIMIRC inhibition alleviated CIH-induced myocardial damage in rats.

In summary, this work demonstrated that circ_CIMIRC silencing repressed FbxL4-mediated ubiquitination and degradation of PINK1 and then enhanced PINK1/Parkin-mediated mitophagy, thereby alleviating myocardial damage in CIH rats. It suggests that modulation of circ_CIMIRC may be a potential strategy to alleviate myocardial damage after CIH.

Limitations of the study

This work has some shortcoming. We constructed OSA mouse model to explore the role of circ_CIMIRC in OSA. However, there were still some differences between OSA mouse model and human OSA conditions. If organoid model can be used, it will be more convinced. Moreover, it is better to collect clinical samples for verification in our future studies.

STAR★METHODS

Detailed methods are provided in the online version of this paper and include the following:

- KEY RESOURCES TABLE
- RESOURCE AVAILABILITY
  - Lead contact
  - Materials availability
  - Data and code availability
- EXPERIMENTAL MODEL AND STUDY PARTICIPANT DETAILS
  - For animal studies
  - For cell lines
- METHOD DETAILS
  - CIH models
  - Histochemical analysis
  - Cell treatment
  - Cell transfection
  - Quantitative real-time PCR (qRT-PCR)
  - Western blotting
  - Ubiquitination assay
  - Cell apoptosis
  - Detection of MDA, SOD and ROS
  - Autophagy flux analysis of LC3B puncta
  - Immunofluorescence (IF) staining
  - Co-Immunoprecipitation (Co-IP) assay
  - RNA immunoprecipitation (RIP)
  - Immunohistochemistry (IHC)
- QUANTIFICATION AND STATISTICAL ANALYSIS

SUPPLEMENTAL INFORMATION

Supplemental information can be found online at https://doi.org/10.1016/j.isci.2024.108982.

ACKNOWLEDGMENTS

This work was supported by National Natural Science Foundation of China (82074192).

AUTHOR CONTRIBUTIONS

Conceptualization: R.W., F.X., and Q.C.; methodology: R.W., F.X., and N.C.; formal analysis: J.L., F.W., and X.W.; writing – original draft: R.W. and F.X.; writing – review and editing: J.L., F.W., and Q.C.; funding acquisition: Q.C. All authors reviewed the whole work and approved the final version of the manuscript.

DECLARATION OF INTERESTS

The authors declare no competing interests.

Received: August 23, 2023
Revised: November 22, 2023
Accepted: January 17, 2024
Published: January 20, 2024

REFERENCES

1. De Backer, W. (2013). Obstructive sleep apnea/hypopnea syndrome. Panminerva Med. *55*, 191–195.
2. Peppard, P.E., Young, T., Barnet, J.H., Palta, M., Hagen, E.W., and Hla, K.M. (2013). Increased prevalence of sleep-disordered breathing in adults. Am. J. Epidemiol. *177*, 1006–1014. https://doi.org/10.1093/aje/kws342.
3. Yang, H., Engeland, C.G., King, T.S., and Sawyer, A.M. (2020). The relationship between diurnal variation of cytokines and symptom expression in mild obstructive sleep apnea. J. Clin. Sleep Med. *16*, 715–723. https://doi.org/10.5664/jcsm.8332.
4. Nácher, M., Serrano-Mollar, A., Farré, R., Panés, J., Seguí, J., and Montserrat, J.M. (2007). Recurrent obstructive apneas trigger early systemic inflammation in a rat model of sleep apnea. Respir. Physiol. Neurobiol. *155*, 93–96. https://doi.org/10.1016/j.resp.2006.06.004.
5. Channaveerappa, D., Lux, J.C., Wormwood, K.L., Heintz, T.A., McLerie, M., Treat, J.A., King, H., Alnasser, D., Goodrow, R.J., Ballard, G., et al. (2017). Atrial electrophysiological and molecular remodelling induced by obstructive sleep apnoea. J. Cell Mol. Med. *21*, 2223–2235. https://doi.org/10.1111/jcmm.13145.
6. Song, J.X., Zhao, Y.S., Zhen, Y.Q., Yang, X.Y., Chen, Q., An, J.R., and Ji, E.S. (2022). Banxia-Houpu decoction diminishes iron toxicity damage in heart induced by chronic intermittent hypoxia. Pharm. Biol. *60*, 609–620. https://doi.org/10.1080/13880209.2022.2043392.
7. Gai, X., Ghezzi, D., Johnson, M.A., Biagosch, C.A., Shamseldin, H.E., Haack, T.B., Reyes, A., Tsukikawa, M., Sheldon, C.A., Srinivasan, S., et al. (2013). Mutations in FBXL4, encoding a mitochondrial protein, cause early-onset mitochondrial encephalomyopathy. Am. J. Hum. Genet. *93*, 482–495. https://doi.org/10.1016/j.ajhg.2013.07.016.
8. Bonnen, P.E., Yarham, J.W., Besse, A., Wu, P., Faqeih, E.A., Al-Asmari, A.M., Saleh, M.A.M., Eyaid, W., Hadeel, A., He, L., et al. (2013). Mutations in FBXL4 cause mitochondrial encephalopathy and a disorder of mitochondrial DNA maintenance. Am. J. Hum. Genet. *93*, 471–481. https://doi.org/10.1016/j.ajhg.2013.07.017.
9. El-Hattab, A.W., Suleiman, J., Almannai, M., and Scaglia, F. (2018). Mitochondrial dynamics: Biological roles, molecular machinery, and related diseases. Mol. Genet. Metab. *125*, 315–321. https://doi.org/10.1016/j.ymgme.2018.10.003.
10. Eicher, J.D., Wakabayashi, Y., Vitseva, O., Esa, N., Yang, Y., Zhu, J., Freedman, J.E., McManus, D.D., and Johnson, A.D. (2016). Characterization of the platelet transcriptome by RNA sequencing in patients with acute myocardial infarction. Platelets *27*, 230–239. https://doi.org/10.3109/09537104.2015.1083543.
11. Ashrafi, G., and Schwarz, T.L. (2013). The pathways of mitophagy for quality control and clearance of mitochondria. Cell Death Differ. *20*, 31–42. https://doi.org/10.1038/cdd.2012.81.
12. Eiyama, A., and Okamoto, K. (2015). PINK1/Parkin-mediated mitophagy in mammalian cells. Curr. Opin. Cell Biol. *33*, 95–101. https://doi.org/10.1016/j.ceb.2015.01.002.
13. Zha, Z., Wang, J., Wang, X., Lu, M., and Guo, Y. (2017). Involvement of PINK1/Parkin-mediated mitophagy in AGE-induced cardiomyocyte aging. Int. J. Cardiol. *227*, 201–208. https://doi.org/10.1016/j.ijcard.2016.11.161.
14. Tu, M., Tan, V., Yu, J., Tripathi, R., Bigham, Z., Barlow, M., Smith, J., Brown, J., and Miyamoto, S. (2022). RhoA signaling increases mitophagy and protects cardiomyocytes against ischemia by stabilizing PINK1 protein and recruiting Parkin to mitochondria. Cell Death and Differ. *29*, 2472–2486. https://doi.org/10.1038/s41418-022-01032-w.
15. Wu, Y., Jiang, T., Hua, J., Xiong, Z., Dai, K., Chen, H., Li, L., Peng, J., Peng, X., Zheng, Z., and Xiong, W. (2022). PINK1/Parkin-mediated mitophagy in cardiovascular disease: From pathogenesis to novel therapy. Int. J. Cardiol. *361*, 61–69. https://doi.org/10.1016/j.ijcard.2022.05.025.
16. Wu, X., Gong, L., Xie, L., Gu, W., Wang, X., Liu, Z., and Li, S. (2021). NLRP3 Deficiency Protects Against Intermittent Hypoxia-Induced Neuroinflammation and Mitochondrial ROS by Promoting the PINK1-Parkin Pathway of Mitophagy in a Murine Model of Sleep Apnea. Front. Immunol. *12*, 628168. https://doi.org/10.3389/fimmu.2021.628168.
17. Xiao, M.S., Ai, Y., and Wilusz, J.E. (2020). Biogenesis and Functions of Circular RNAs Come into Focus. Trends Cell Biol. *30*, 226–240. https://doi.org/10.1016/j.tcb.2019.12.004.
18. Zhang, T.R., and Huang, W.Q. (2020). Angiogenic circular RNAs: A new landscape in cardiovascular diseases. Microvasc. Res. *129*, 103983. https://doi.org/10.1016/j.mvr.2020.103983.
19. Zhang, Z., Zhang, T., Feng, R., Huang, H., Xia, T., and Sun, C. (2019). circARF3 Alleviates Mitophagy-Mediated Inflammation by Targeting miR-103/TRAF3 in Mouse Adipose Tissue. Molecular therapy. Nucleic Acids *14*, 192–203. https://doi.org/10.1016/j.omtn.2018.11.014.
20. El-Hattab, A.W., Craigen, W.J., and Scaglia, F. (2017). Mitochondrial DNA maintenance defects. Biochim. Biophys. Acta Mol. Basis Dis. *1863*, 1539–1555. https://doi.org/10.1016/j.bbadis.2017.02.017.
21. Schwemmlein, J., Maack, C., and Bertero, E. (2022). Mitochondria as Therapeutic Targets in Heart Failure. Curr. Heart Fail. Rep. *19*, 27–37. https://doi.org/10.1007/s11897-022-00539-0.
22. Yapa, N.M.B., Lisnyak, V., Reljic, B., and Ryan, M.T. (2021). Mitochondrial dynamics in health and disease. FEBS Lett. *595*, 1184–1204. https://doi.org/10.1002/1873-3468.14077.
23. Ji, Y., Leng, Y., Lei, S., Qiu, Z., Ming, H., Zhang, Y., Zhang, A., Wu, Y., and Xia, Z. (2022). The mitochondria-targeted antioxidant MitoQ ameliorates myocardial ischemia-reperfusion injury by enhancing PINK1/Parkin-mediated mitophagy in type 2 diabetic rats. Cell Stress Chaperones *27*, 353–367. https://doi.org/10.1007/s12192-022-01273-1.
24. Yang, X., Zhou, Y., Liang, H., Meng, Y., Liu, H., Zhou, Y., Huang, C., An, B., Mao, H., and Liao, Z. (2021). VDAC1 promotes cardiomyocyte autophagy in anoxia/reoxygenation injury via the PINK1/Parkin pathway. Cell Biol. Int. *45*, 1448–1458. https://doi.org/10.1002/cbin.11583.
25. Zhou, J., Wang, Z., He, Y., Luo, X., Zhang, W., Yu, L., Chen, X., He, X., Yuan, Y., Wang, X., et al. (2020). Qiliqiangxin reduced cardiomyocytes apotosis and improved heart function in infarcted heart through Pink1/Parkin -mediated mitochondrial autophagy. BMC Complement. Med. Ther. *20*, 203. https://doi.org/10.1186/s12906-020-02992-7.
26. Varshavsky, A. (2017). The Ubiquitin System, Autophagy, and Regulated Protein Degradation. Annu. Rev. Biochem. *86*, 123–128. https://doi.org/10.1146/annurev-biochem-061516-044859.
27. Peng, J., Song, J., Zhou, J., Yin, X., and Song, J. (2019). Effects of CPAP on the transcriptional signatures in patients with obstructive sleep apnea via coexpression network analysis. J. Cell. Biochem. *120*, 9277–9290. https://doi.org/10.1002/jcb.28203.

28. Li, H., Xu, J.D., Fang, X.H., Zhu, J.N., Yang, J., Pan, R., Yuan, S.J., Zeng, N., Yang, Z.Z., Yang, H., et al. (2020). Circular RNA circRNA_000203 aggravates cardiac hypertrophy via suppressing miR-26b-5p and miR-140-3p binding to Gata4. Cardiovasc. Res. *116*, 1323–1334. https://doi.org/10.1093/cvr/cvz215.

29. Garikipati, V.N.S., Verma, S.K., Cheng, Z., Liang, D., Truongcao, M.M., Cimini, M., Yue, Y., Huang, G., Wang, C., Benedict, C., et al. (2019). Circular RNA CircFndc3b modulates cardiac repair after myocardial infarction via FUS/VEGF-A axis. Nat. Commun. *10*, 4317. https://doi.org/10.1038/s41467-019-11777-7.

30. Lai, S., Chen, L., Zhan, P., Lin, G., Lin, H., Huang, H., and Chen, Q. (2021). Circular RNA Expression Profiles and Bioinformatic Analysis in Mouse Models of Obstructive Sleep Apnea-Induced Cardiac Injury: Novel Insights Into Pathogenesis. Front. Cell Dev. Biol. *9*, 767283. https://doi.org/10.3389/fcell.2021.767283.

STAR★METHODS

KEY RESOURCES TABLE

REAGENT or RESOURCE	SOURCE	IDENTIFIER
Antibodies		
rabbit anti-FbxL4	Bioss	Cat#bs-13166R
rabbit anti-PINK1	Proteintech,	Cat#23274-1-AP; RRID: AB_2879244
mouse anti-Parkin	Thermo Fisher Scientific	Cat#39-0900; RRID: AB_2533396
rabbit anti-LC3	Proteintech	Cat#14600-1-AP; RRID: AB_2137737
rabbit anti-cleaved caspase-3	Thermo Fisher Scientific	Cat#PA5-114687; RRID: AB_2899323
rabbit anti-p62	Abcam	Cat#ab240635; RRID: AB_2885121
rabbit anti-Bcl-2	Abcam	Cat#ab196495; RRID: AB_292486
rabbit anti-Mfn2	Abcam	Cat#ab124773; RRID: AB_10999860
rabbit anti-Drp1	Abcam	Cat#ab184247; RRID: AB_2895215
rabbit anti-GAPDH	Abcam	Cat#ab181602; RRID: AB_2630358
rabbit anti-β-actin	Abcam	Cat#ab8227; RRID: AB_2305186
goat anti-mouse IgG	Abcam	Cat#ab6789; RRID: AB_955439
goat anti-rabbit IgG	Abcam	Cat#ab6721; RRID: AB_955447
anti-ubiquitin	Abcam	Cat#ab134953; RRID: AB_2801561
anti-Tom20	Thermo Fisher Scientific	Cat#PA5-52843; RRID: AB_2648808
mouse anti-Parkin	Thermo Fisher Scientific	Cat#39-0900; RRID: AB_2533396
donkey anti-rabbit IgG-Alexa Fluor™ 647	Thermo Fisher Scientific	Cat#A-31573; RRID: AB_2536183
goat anti-mouse IgG-FITC	Thermo Fisher Scientific	Cat#F-2761; RRID: AB_2536524
Chemicals, peptides, and recombinant proteins		
DMEM	GIBCO	Cat#11960044
Fetal bovine serum	GIBCO	Cat#16140071
MG132	MedChem Express	Cat#HY-13259
Mdivi-1	MedChem Express	Cat#HY-15886
DMSO	MedChem Express	Cat#HY-Y0320
Lipofectamine 2000 Reagent	Thermo Fisher Scientific	Cat#11668500
Lipofectamine™ RNAiMAX	Thermo Fisher Scientific	Cat#13778100
TRIzol reagent	Thermo Fisher Scientific	Cat#15596026
RIPA buffer	Thermo Fisher Scientific	Cat#89901
DAPI	Beyotime	Cat#C1002
DAB	Biogradetech	Cat#B-IMWRS51-100T
Critical commercial assays		
One Step TUNEL Apoptosis Assay Kit	Beyotime	Cat#C1086
MDA assay kit (TBA method)	Nanjing Jiancheng Biological Engineering Research Institute	Cat#A003-1-2
ROS Assay Kit	Nanjing Jiancheng Biological Engineering Research Institute	Cat#E004-1-1
SOD assay kit (WST-1 method)	Nanjing Jiancheng Biological Engineering Research Institute	Cat#A001-3-2
Ad-GFP-LC3B	Beyotime	Cat#C3006
Protein A Agarose beads	Cell Signaling Technology	Cat#9863
Magna RIP RNA-Binding Protein Immunoprecipitation Kit	Millipore	Cat#17-700

(*Continued on next page*)

Continued

REAGENT or RESOURCE	SOURCE	IDENTIFIER
Hematoxylin and Eosin Staining Kit	Beyotime	Cat#C0105M
Masson Staining Kit	SenBeiJia	Cat#BP-DL021
Colorimetric TUNEL Apoptosis Assay Kit	Beyotime	Cat#C1091
Cytoplasm and Nuclear RNA Purification Kit	Norgen Biotek	Cat#21000
TransScript® One-Step gDNA Removal and cDNA Synthesis SuperMix	Transgen	Cat#AQ601-01-V2
PerfectStart® Green qPCR SuperMix	Transgen	Cat#AQ601-01-V2
Experimental models: Cell lines		
H9c2 cells	ATCC	Cat#CRL-1446; RRID: CVCL_0286
Experimental models: Organisms/strains		
Sprague Dawley male rats	Hangzhou Medical College	N/A
Software and algorithms		
ImageJ Software	National Institutes of Health	https://imagej.nih.gov/ij
GraphPad Prism 9.0	GraphPad Prism Software	https://www.graphpad.com/
SPSS 22.0 statistical software	IBM Corp.	https://www.ibm.com/products/spss-statistics

RESOURCE AVAILABILITY

Lead contact

Further information and requests for resources and reagents should be directed to the lead contact, Qin Chen (2014015@fjtcm.edu.cn).

Materials availability

Requests for materials should be directed to the corresponding authors.

Data and code availability

Data reported in this paper and additional information required to reanalyze the data reported in the study are available from the lead contact upon request.

This paper does not report any original code.

EXPERIMENTAL MODEL AND STUDY PARTICIPANT DETAILS

For animal studies

Sprague Dawley (SD) male rats (6 weeks old, weighing 180 ± 20 g) were obtained from Hangzhou Medical College (Hangzhou, China). Rats were housed under SPF conditions. This study was authorized by the Ethics Committee of Fujian University of Traditional Chinese Medicine (No. FJTCM IACUC 2021162).

For cell lines

H9c2 cells (ATCC, Manassas, VA, USA) were cultured in DMEM (GIBCO, Grand Island, NY, USA) containing 10% fetal bovine serum (GIBCO) at 37°C and 5%CO_2.

METHOD DETAILS

CIH models

Animal model of CIH was constructed. Rats were randomly divided into 4 groups (n = 8): (1) Normal group: rats were received 21% O_2 for 24 h/day, 8 weeks. (2) CIH group: rats were received CIH treatment for 8 h/day, 8 weeks. (3) sh-CIMIRC group: rats were received CIH treatment, and then injected with lentivirus (LV)-mediated shRNA specifically targeting circ_CIMIRC (sh-CIMIRC) into caudal vein. (4) sh-NC group: rats were received CIH treatment, and then injected with lentivirus (LV)-mediated scrambled shRNA (sh-NC) into caudal vein. Rats were subjected to CIH treatment in an Animal intermittent hypoxia incubator (Attendor-140 Pro, Ningbo, China) with 5.1-21% O_2. The CIH cycle was contained 4 periods: (1) oxygen concentration decline period (50 s); (2) hypoxic maintenance period (20 s); (3) oxygen concentration rise period (30 s); (4) normoxic maintenance period (20 s). Each cycle lasted for 120 s, and run 30 times/hour. After modeling, hearts were separated

from euthanized rats and weighed. The ratio of heart weight/body weight (HW/BW) was calculated. Subsequently, myocardial tissues were obtained for further use.

Histochemical analysis

Following of fixation and embedding, paraffin sections of myocardial tissues were obtained. Myocardial tissue sections were stained with Hematoxylin and Eosin Staining Kit (Beyotime, Shanghai, China). The pathology injury score of myocardial tissues was evaluated following the scoring criteria: (1) 0 point: no injury; (2) 1 point: minor injury, focal myocardial cell injury or degeneration; (3) 2 point: moderate injury, extensive myofibrillar degeneration, swelling, inflammatory cell infiltration; (4) 3 point: severe injury, diffuse necrosis, swelling, degeneration, massive inflammatory cell infiltration. Masson Staining Kit (SenBeiJia, Nanjing, China) and Colorimetric TUNEL Apoptosis Assay Kit (Beyotime) were used to assess the fibrosis and apoptosis of myocardial tissues as the manufacturer's instructions. The collagen volume fraction (CVF) and TUNEL positive cells in myocardial tissues were calculated.

Cell treatment

Cells were received CIH treatment (repeated cycles of 21% O_2 for 5 min; followed by 5% O_2 for 5 min) (Smartor-118pro , Ningbo, China) for 24 h. Cells incubated in normoxia conditions served as control. Cells were treated with 25 μM of MG132 (proteasome inhibitor; dissolved in DMSO; MedChem Express, Monmouth Junction, NJ, USA) for 8 h or treated with 50 μM of Mdivi-1 (mitochondrial fission inhibitor; MedChem Express) for 1 h. Cells were treated with DMSO as control.

Cell transfection

For overexpression of FbxL4 or circ_CIMIRC, the pcDNA3.1 vector carrying FbxL4 (pcDNA-FbxL4) or circ_CIMIRC (pcDNA-CIMIRC) was constructed. SiRNA specifically targeting FbxL4 (si-FbxL4) or circ_CIMIRC (si-circ_CIMIRC) was synthesized. Empty vector (pcDNA-NC) and scrambled siRNA (si-NC) served as control. All these vectors were obtained from GenePharma (Shanghai, China). H9c2 cells were transfected with vectors or siRNAs utilizing Lipofectamine 2000 Reagent (Thermo Fisher Scientific, Waltham, MA, USA) or Lipofectamine™ RNAiMAX (Thermo Fisher Scientific).

Quantitative real-time PCR (qRT-PCR)

Cytoplasm, nuclear and total RNAs were isolated from H9c2 cells and myocardial tissues applying TRIzol reagent (Thermo Fisher Scientific) and Cytoplasm and Nuclear RNA Purification Kit (Norgen Biotek, St. Catherines, Canada). RNA samples were sun on agarose gel electrophoresis for quality test. Complementary DNA synthesis and PCR reactions were performed utilizing TransScript® One-Step gDNA Removal and cDNA Synthesis SuperMix and PerfectStart® Green qPCR SuperMix (Transgen, Beijing, China). Gene expression was normalized to GAPDH and analyzed by $2^{-\Delta\Delta Ct}$ method.

Western blotting

H9c2 cells and myocardial tissues were lysed with RIPA buffer (Thermo Fisher Scientific), total proteins were extracted from the lysis solution. Applying 10% SDS-PAGE gel electrophoresis, protein samples were separated. The separated proteins were transferred to PVDF membranes, and then incubated sequentially with primary antibodies and secondary antibody. The antibodies used in western blotting shown as follows: rabbit anti-FbxL4 (1:1000; bs-13166R; Bioss, Beijing, China), rabbit anti-PINK1 (1:500; 23274-1-AP; Proteintech, Wuhan, China), mouse anti-Parkin (1:500; 39-0900; Thermo Fisher Scientific), rabbit anti-LC3 (1:1000; 14600-1-AP; Proteintech), rabbit anti-cleaved caspase-3 (1:1000; PA5-114687; Thermo Fisher Scientific), rabbit anti-p62 (1:1000; ab240635; Abcam, Cambridge, MA, USA), rabbit anti-Bcl-2 (1:1000; ab196495; Abcam), rabbit anti-Mfn2 (1:1000; ab124773; Abcam), rabbit anti-Drp1 (1:1000; ab184247; Abcam), rabbit anti-GAPDH (1:10000; ab181602; Abcam), rabbit anti-β-actin (1:1000; ab8227; Abcam), goat anti-mouse IgG (1:5000; ab6789; Abcam), goat anti-rabbit IgG (1:10000; ab6721; Abcam). The immunoreactive bands were visualized by enhanced chemiluminescence reagent.

Ubiquitination assay

H9c2 cells and myocardial tissues were lysed with RIPA buffer containing protease inhibitor. Cell lysates were incubated with anti-PINK1 and then treated with Protein A+G Agarose beads (Cell Signaling Technology, Danvers, MA, USA). The bead-antigen-antibody complex was eluted from the cell lysates. The bead-protein complex was separated on 10% SDS-PAGE gel, and then used for western blotting with anti-ubiquitin (1:1000; ab134953; Abcam). For site-directed mutagenesis, the mutation sites of PINK1 (K267, K319, K369, K433, K458, K496) were constructed to replace the lysines with arginines (GenePharma). H9c2 cells were transfected with wild type and mutant of PINK1 ubiquitination sites (WT-K267, MUT-K267, WT-K319, MUT-K319, WT-K369, MUT-K369, WT-K433, MUT-K433, WT-K458, MUT-K458, WT-K496 and MUT-K496). Then, the levels of PINK1 ubiquitination were analyzed.

Cell apoptosis

One Step TUNEL Apoptosis Assay Kit (Beyotime) were used to examine apoptotic cells as the instructions of manufacturer. Cells were incubated with TUNEL reagent at 37°C for 1 h, and then counterstained with DAPI (Beyotime). The fluorescence of cells was observed applying fluorescence microscope (Olympus, Tokyo, Japan).

Detection of MDA, SOD and ROS

The levels of malondialdehyde (MDA), superoxide dismutase (SOD) and ROS in myocardial tissues were examined applying MDA assay kit (TBA method), ROS Assay Kit and SOD assay kit (WST-1 method) (Nanjing Jiancheng Biological Engineering Research Institute, Nanjing, China) according to the protocols of manufacturer.

Autophagy flux analysis of LC3B puncta

H9c2 cells were cultured to 50–70% confluence in 6-well plates. Then, cells were infected with Ad-GFP-LC3B (Beyotime) applying polybrene. The GFP-LC3B puncta (green fluorescence) was observed under a fluorescence microscope.

Immunofluorescence (IF) staining

H9c2 cells were seeded onto coverslips and allowed to reach 70% confluency. After washing with PBS, cells were fixed with 4% paraformaldehyde and treated with 0.5% Triton X-100. Cells were then blocked with bovine serum albumin (BSA). After that, cells were incubated with rabbit anti-Tom20 (PA5-52843; Thermo Fisher Scientific) or mouse anti-Parkin (39-0900; Thermo Fisher Scientific). Then, cells were incubated with donkey anti-rabbit IgG-Alexa Fluor™ 647 (A-31573; Thermo Fisher Scientific) or goat anti-mouse IgG-FITC (F-2761; Thermo Fisher Scientific). Cell nucleus were stained with DAPI. Colocalization of Tom20 and Parkin was observed under a fluorescence microscope.

Co-Immunoprecipitation (Co-IP) assay

H9c2 cells were lysed with RIPA buffer. The cell lysis solution was incubated with anti-FbxL4 or anti-PINK1 at 4°C overnight. Cell lysis solution served as input group. Subsequently, cell lysis solution was treated with Protein A Agarose beads (Cell Signaling Technology) at 4°C. After 2 hours of incubation, the liquid supernatant was obtained from the cell lysis solution by centrifugation. After washing with PBS for several times, the captured protein precipitation was run on 10% SDS gel. The separated proteins were subjected to western blotting applying anti-FbxL4 or anti-PINK1 antibodies.

RNA immunoprecipitation (RIP)

RIP was performed applying Magna RIP RNA-Binding Protein Immunoprecipitation Kit (Millipore, Darmstadt, Germany) to examine the relationship among circ_CIMIRC, FbxL4 and PINK1. Cells were lysed with RIPA buffer. The cell supernatant was incubated with anti-FbxL4, anti-PINK1 or anti-IgG for coprecipitation, and then incubated with magnetic beads. After that, the magnetic bead-antibody complex was collected applying magnetic stand. The proteins were digested with proteinase K. Finally, the RNA was extracted for qRT-PCR analysis.

Immunohistochemistry (IHC)

Paraffin of myocardial tissues were treated with H_2O_2 and sodium citrate for antigen retrieval. Then, sections were blocked with BSA. Sections were successively incubated with anti-FbxL4, and anti-IgG. sections were stained with DAB (Biogradetech, Wuhan, China), and then counterstained with hematoxylin. Finally, the sections were observed under microscope.

QUANTIFICATION AND STATISTICAL ANALYSIS

All data were expressed mean ± SEM and obtained from 3 independent experiments. Statistical calculations were conducted utilizing GraphPad Prism 9.0 and SPSS 22.0 statistical software (IBM, Armonk, NY, USA). Two-tailed Student's *t* test and one-way ANOVA were conducted to analysis the statistical difference. $P < 0.05$ was considered significant.